MEASUREMENT OF DUST OPTICAL PROPERTIES IN COALSACK

N. V. SUJATHA, JAYANT MURTHY, P. SHALIMA

sujaskm@yahoo.co.in, jmurthy@yahoo.com, shalima.p@gmail.com

Indian Institute of Astrophysics, Koramangala, Bangalore - 560 034, India

and

RICHARD CONN HENRY

henry@jhu.edu

Dept. of Physics and Astronomy

The Johns Hopkins University, Baltimore, MD 21218

ABSTRACT

We have used *FUSE* and *Voyager* observations of dust scattered starlight in the neighborhood of the Coalsack Nebula to derive the optical constants of the dust grains. The albedo is consistent with a value of 0.28 ± 0.04 and the phase function asymmetry factor with a value of 0.61 ± 0.07 throughout the spectral range from 900 – 1200 Å, in agreement with previous determinations as well as theoretical predictions. We have now observed *two* regions (Ophiuchus and Coalsack) with intense diffuse background radiation and in both cases have found that the emission is due to light from nearby hot stars scattered by a relatively thin foreground cloud, with negligible contribution from the background molecular cloud.

Subject headings: ultraviolet: ISM — dust, extinction

1. INTRODUCTION

It has long been assumed that the diffuse far-ultraviolet (FUV) background should be correlated with the amount of H I in the line of sight (e.g., Maucherat-Joubert et al. 1980). While this may be true at high galactic latitudes where Haikala et al. (1995) and

Schiminovich et al. (2001) have both found the UV scattered light to be correlated with the 100 μm emission observed using the *Infrared Astronomical Satellite* (*IRAS*), albeit with different correlation factors, it is now becoming apparent that local effects, such as the proximity of dust to hot stars, can also play an important role in the level of the diffuse UV background (Murthy & Sahnow 2004; Edelstein et al. 2006). This interdependence is even more apparent in the LMC where Cole et al. (1999) have found that neither bright stars nor dust are sufficient in themselves to produce scattered emission; only when both are present with a favourable geometry is scattered light seen. In our own Galaxy, Lee et al. (2006) found the scattered radiation in Taurus to be actually anti-correlated with the gas column density suggesting that the source of the radiation is behind the molecular cloud.

In addition to characterizing and understanding the diffuse radiation field, one of our scientific goals has been to extract the optical constants – the albedo (a) and phase function asymmetry factor (g) – of the interstellar dust grains. This has been complicated by the faintness of the signal and lack of knowledge about the scattering geometry (Mathis et al. 2002). Thus, although we have observed targets over the entire sky (Murthy et al. 1999; Murthy & Sahnow 2004), we have chosen to begin our modeling with two regions where the signal is bright and the interstellar dust distribution, from whence the scattering comes, is well characterized. The first of these was in the constellation of Ophiuchus (Sujatha et al. 2005) and the second, which we present here, is near the Coalsack Nebula.

Murthy et al. (1994) found from observations made with the two *Voyager* Ultraviolet Spectrographs (UVS) that the Coalsack was one of the brightest regions of diffuse UV emission in the sky and they attributed this emission to forward scattering from a relatively thin H I cloud in front of the Coalsack molecular cloud, a conclusion later confirmed by Shalima & Murthy (2004). In order to supplement these observations, we searched for further observations made with the *Far Ultraviolet Spectroscopic Explorer* (*FUSE*) finding an additional 29 observations of 21 targets, including 3 observations that were made as part of our own *FUSE* guest investigator observing program.

2. OBSERVATIONS

We have collected 34 observations (29 from *FUSE* and 5 from the *Voyager* UVS) of the diffuse radiation in and around the Coalsack Nebula (Table 1). Of the five observations made with the *Voyager* UVS, four have already been discussed by Murthy et al. (1994) and a full description of the instrument and diffuse observations made with it has been given by Murthy et al. (1999) and references therein. Briefly, the *Voyager* UVS observe diffuse radiation from 500 - 1600 Å with a resolution of about 38 Å. The field of view is large

($0.1^\circ \times 0.87^\circ$) and integration times are long resulting in a sensitivity to diffuse radiation of better than 100 photons cm^{-2} sr^{-1} s^{-1} Å^{-1}.

The remaining 29 observations were made with the LWRS ($30'' \times 30''$) aperture on the *FUSE* spacecraft. The four *FUSE* spectrographs cover the wavelength region from 850 - 1167 Å with a resolution ($\lambda/\Delta\lambda$) of about 20000. Although intended for observations of point sources (see Moos et al. 2000; Sahnow et al. 2000, for a description of the spacecraft and mission), Murthy & Sahnow (2004) have shown that background levels of 2000 photons cm^{-2} sr^{-1} s^{-1} Å^{-1} are detectable with the LWRS aperture.

Following Murthy & Sahnow (2004), we binned the data into broad bands of about 50 Å in width in order to increase the signal-to-noise ratio. This yields a total of 6 independent bands (Table 2) with sufficient sensitivity to detect the diffuse radiation from the Coalsack. Because the 2A2 and 1B1 bands and the 2A1 and 1B2 bands, respectively, had similar bandpasses, we used their weighted average for our further calculations. A point source in the aperture will result in a Gaussian with a width of about 18 pixels while a diffuse aperture filling source will yield a Gaussian with a width of 30 pixels. We have used this width to ensure that the signal in our observations was indeed of diffuse origin.

We have additionally searched the Digital Sky Survey plates from CDS[1] and found no point sources in the aperture. However, it is interesting to calculate the brightness of a star whose contribution would be equivalent to a diffuse flux of 20,000 photons cm^{-2} sr^{-1} s^{-1} Å^{-1}. A star with a spectral type of later than about B9 would simply not have enough flux to contribute in the *FUSE* range without being blazingly bright in the visible. On the other hand, this amount of diffuse flux corresponds to an unreddened 18^{th} magnitude B3 star implying a spectroscopic distance of about 1.5 kpc, or well beyond the Coalsack Nebula which would, of course, absorb any UV component of such a star.

Our observed values for each of the 6 *FUSE* bands and for the *Voyager* spectra at the same wavelengths are listed in Table 1 and are superimposed on a 100 μm map from *IRAS* in Fig. 1. The circles are centred on the observed locations and the diameter of each circle is proportional to the weighted average of the intensity in the 2A2 and 1B1 bands at an effective wavelength of about 1114 Å.

---

[1]Centre de Donnes astronomiques de Strasbourg : http://cdsweb.u-strasbg.fr/

3. RESULTS AND MODELING

It is apparent from Fig. 1 and Fig. 2, where the weighted average of the 2A2 and 1B1 bands are plotted against the 100 μm intensity, that there is not a simple correlation between the UV and IR emission. There is a tendency for the amount of diffuse UV light to increase with the IR emission up to an intensity of about 80 MJy sr^{-1}, but with a lot of scatter. This correlation breaks down for larger IR intensities possibly suggesting that both the IR and UV emission are dominated by emission from the foreground cloud at lower H I column densities (as traced by the IR) but not at higher column densities where the IR emission is largely due to emission from dust in the optically thick Coalsack molecular cloud.

The scattered UV light from any location in space is a function of the interstellar radiation field (ISRF), the amount of dust in the line of sight and the scattering function of the dust grains. Of these, the ISRF is the easiest to derive as the Coalsack is so thick that no stars will be seen from behind the cloud, particularly in the UV, and the radiation field is dominated by only 13 stars (Table 3). As described by Sujatha et al. (2004) we have used the Hipparcos catalog to locate the stars in 3-dimensions and calculated their contribution at the location of scattering based on their spectral type, V magnitude, and appropriate Kurucz models (Kurucz 1992). Not less than 95% of the total ISRF in the vicinity of the Coalsack comes from these stars. This method is identical to that of Shalima & Murthy (2004) except that they had incorrectly scaled the FUV fluxes of the stars to observations made with the small aperture of the *International Ultraviolet Explorer*. The small aperture of *IUE* is known to underestimate stellar fluxes by about 40% and thus they derived an albedo that was too high by the same factor. The FUV fluxes used in this work are in agreement with large aperture *IUE* observations of the stars.

The dust distribution has been well characterized by Corradi et al. (2004) using 4 color photometry of several hundred stars in the region. They have found, in addition to the Coalsack Nebula itself at a distance of 180 pc, two foreground clouds of neutral hydrogen at distances of 60 pc and 120 - 150 pc. The column densities (N(H I)) of these clouds are 3.2 $\times$ 10^{19} cm^{-2} and 1.5 $\times$ 10^{21} cm^{-2}, respectively. We have used all three clouds in our modeling but note that most of the observed light comes from the more distant of the two H I clouds.

We have implemented a Monte Carlo code to account for multiple scattering in all three clouds: the two foreground neutral hydrogen clouds and the Coalsack molecular cloud. In this code, a photon is emitted in a random direction from one of the stars and continues in a straight line until it has an interaction with a dust grain, the probability of which depends on the local density and the grain cross-section, taken from the "Milky Way" model of Weingartner & Draine (2001). This model uses a mixture of silicate and graphite grains with implicit assumptions of $R_V = 3.1$ and the canonical gas-to-dust ratio of Bohlin et al.

(1978). After each interaction, the relative weight of the photon is reduced by the albedo and it is scattered into a new direction with a probability taken from the Henyey-Greenstein scattering function (Henyey & Greenstein 1941). Each individual photon is followed either until its weight becomes negligible or the photon escapes the region of interest. A complete run consists of about 10^7 photons emitted for each star for each value of a and g.

We found that most of the observed radiation arose in the more distant of the two foreground clouds and hence most of the uncertainty in our model results comes from the uncertainty in the actual distance of that cloud. Because there is no reason to assume that the cloud is flat and perpendicular to our line of sight, we have derived the distance at each scattering location by finding the combination of optical constants (a and g) and distance which gives the best match of the predicted light with the observed value (weighted average of the 2A2 and 1B1 bands, i.e., at 1114 Å), with the further assumption that the optical constants are the same throughout the region. These distances are plotted in Fig. 3 with error bars showing the range of allowed distances. Any point outside this allowed region will not satisfy our conditions of uniform a and g. Given the sparse nature of our data, we find a contiguous but warped cloud.

Our final model assumes three clouds each with a 1 pc thickness (defined by our bin size): the Coalsack molecular cloud at a distance of 180 pc, a cloud of neutral hydrogen at a distance of 60 pc from the Sun, and the cloud illustrated in Fig. 3b with a distance at each point as found from the best fit to the data. The output of this model is an image of the region around the Coalsack for each value of the optical constants which can be directly compared to the observations in each of the wavelength bands. Fig. 4 shows this image for the best fit values of a and g (0.28 and 0.61, respectively) at a wavelength 1114 Å, with our observations plotted as circles whose diameters are proportional to the weighted average of the 2A2 and 1B1 bands.

The 6 *FUSE* bands (Table 2) allowed observations at 4 wavelengths (1004 Å, 1058 Å, 1114 Å, and 1158 Å) where the intensities at 1114 Å and 1158 Å were taken from the weighted average of the 2A2 and 1B1 bands and 2A1 and 1B2 bands, respectively. The *Voyager* UVS is far more sensitive to diffuse radiation because of its relatively large aperture and allowed observation of the entire spectrum of the diffuse radiation between 912 Å (the Lyman limit) and 1200 Å.

Our predictions from our best fit model agree well with the observations both spatially (Fig. 5) and spectrally (Fig. 6). We have plotted 67% and 95% confidence contours (following the procedure of Lampton et al. (1976)) for a and g in Fig. 7. They are consistent with values of 0.28 ± 0.04 for the albedo and 0.61 ± 0.07 for the phase function asymmetry factor throughout the spectral range from 912 Å to 1200 Å (Fig. 8), in agreement with the

prediction of Weingartner & Draine (2001) for their "Milky Way" model. The error bars in the optical constants include both observational errors and errors in the modeling, such as in the distance.

4. CONCLUSIONS

We have used *Voyager* and *FUSE* observations of diffuse emission near the Coalsack Nebula to constrain the optical parameters of the interstellar dust. We find that the albedo a is 0.28 ± 0.04 and g is 0.61 ± 0.07 throughout the spectral range from 900 to 1200 Å. These values are consistent with previous determinations in reflection Nebulae (Witt et al. 1993; Burgh et al. 2002), in diffuse clouds (Sujatha et al. 2005), and in Orion (Shalima et al. 2006). It is clear that interstellar grains in the FUV are strongly forward scattering with a moderately low albedo, in agreement with theoretical prediction for a mixture of graphite and silicate grains (Weingartner & Draine 2001). Even though small grains have been depleted in Orion ($R_V = 5.5$; Fitzpatrick (1999)), it makes little difference to the optical constants (Weingartner & Draine 2001) and our data cannot distinguish between them.

It had been our hope that we could derive a global model for the diffuse UV radiation over the entire sky. However, we have found the true situation to be more complex with the radiation being dependent largely on the presence of scattering dust near a hot star. In particular, we note that the *SPEAR* data (Edelstein et al. 2006) show strong enhancements in the diffuse emission in the Ophiuchus and Coalsack regions which one might have naively associated with the prominent molecular clouds in those regions. However, our detailed modeling (Sujatha et al. (2005) and this paper, respectively) have shown that the emission is actually due to scattering from a much thinner foreground cloud. We plan to continue our characterization of the diffuse UV radiation field and its implications for the nature of the interstellar dust using *Voyager*, *FUSE* and *GALEX* (*Galaxy Evolution Explorer*) observations.

We thank an anonymous referee for constructive criticism which we hope has resulted in a better paper. We thank the *FUSE* team for much helpful information and discussion. This research has made use of NASA's Astrophysics Data System and the SIMBAD database operated at CDS, Strasbourg, France. The data presented in this paper were obtained from the Multimission Archive at the Space Telescope Science Institute (MAST). STScI is operated by the Association of Universities for Research in Astronomy, Inc. under NASA contract NAS5-26555. Support for MAST for non-HST data is provided by the NASA Office of Space Science via grant NAG5-7584 and by other grants and contracts.

REFERENCES

Bohlin, R. C., Savage, B. D., & Drake, J. F. 1978, ApJ, 224, 132

Burgh, E. B., McCandliss, S. R., & Feldman, P. D. 2002, ApJ, 575, 240

Cole, A. A., Wood, K., & Nordsieck, K. H. 1999, AJ, 118, 2292

Corradi, W. J. B., Franco, G. A. P., & Knude, J. 2004, MNRAS, 347, 1065

Edelstein, J., et al. 2006, ApJ, 644, 153

Fitzpatrick, E. L. 1999, PASP, 111, 63

Haikala, L. K., Mattila, K., Bowyer, S., Sasseen, T. P., Lampton, M., & Knude, J. 1995, ApJ, 443, 33

Henyey, L. C., & Greenstein, J. L. 1941, ApJ, 93, 70

Kurucz, R. L. 1992, in The Stellar Populations of Galaxies, IAU Symp., 149, ed. B. Barbuy & A. Renzini (Dordrecht: Kluwer), 225

Lampton, M., Margon, B., & Bowyer, S. 1976, ApJ, 208, 177

Lee, D. H., et al. 2006, ApJ, 644, L181

Mathis, J. S., Whitney, B. A., & Wood, K. 2002, ApJ, 574, 812

Maucherat-Joubert, M., Deharveng, J. M., & Cruvellier, P. 1980, A&A, 88, 323

Moos, H. W., et al. 2000, ApJ, 538, 1

Murthy, J., Hall, D., Earl, M., Henry, R. C., & Holberg, J. B. 1999, ApJ, 522, 904

Murthy, J., Henry, R. C., & Holberg, J. B. 1994, ApJ, 428, 233

Murthy, J., & Sahnow, D. J. 2004, ApJ, 615, 315

Perryman, M. A. C., et al. 1997, A&A, 323, 49

Sahnow, D. J., et al. 2000, ApJ, 538, 7

Schiminovich, D., Friedman, P. G., Martin, C., & Morrissey, P. F. 2001, ApJ, 563, 161

Shalima, P., & Murthy, J. 2004, MNRAS, 352, 1319

Shalima, P., Sujatha, N. V., Murthy, J., Henry, R. C., & Sahnow, D. J. 2006, MNRAS, 367, 1686

Sujatha, N. V., Chakraborty, P., Murthy, J., & Henry, R. C. 2004, BASI, 32, 151

Sujatha, N. V., Shalima, P., Murthy, J., & Henry, R. C. 2005, ApJ, 633, 257

Weingartner, J. C., & Draine, B. T. 2001, ApJ, 548, 296

Witt, A. N., Petersohn, J. K., Holberg, J. B., Murthy, J., Dring, A., & Henry, R. C. 1993, ApJ, 410, 714

Table 1. OBSERVED LOCATIONS IN THE COALSACK

No.	Data ID	Target Name	l (deg)	b (deg)	Observed UV Intensity ± Error (photons cm^{-2} s^{-1} sr^{-1} Å^{-1}) 1A1 (1004 Å)	1A2 (1058 Å)	2A2 (1112 Å)	1B1 (1117 Å)	1B2 (1157 Å)	2A1 (1159 Å)	IR 100 μm (MJy sr^{-1})
1	Voyager 1[a]	BKGND3	301.7	-1.7	13165 ± 366	16212 ± 590	17023 ± 730	18500 ± 800	23675 ± 1500	23700 ± 1500	123
2	Voyager 2[b]	Coalsack	303.7	0.8	9240 ± 1000	10750 ± 545	13950 ± 2000	11519 ± 700	15120 ± 800	15210 ± 1000	343
3	Voyager 3[b]	Coalsack	303.7	0.8	10880 ± 700	13815 ± 700	14000 ± 2300	13823 ± 700	15916 ± 1200	14104 ± 800	343
4	Voyager 4[b]	Coalsack	304.6	-0.4	4311 ± 500	6140 ± 500	11900 ± 2400	8295 ± 500	11150 ± 800	11000 ± 1000	400
5	Voyager 5[b]	Coalsack	305.2	-5.7	9450 ± 500	11060 ± 700	8000 ± 2000	11520 ± 1000	16720 ± 1200	15500 ± 1500	35
6	B0680101	Gamma-Cru	300.17	5.65	1045 ± 792	3077 ± 825	3031 ± 518	289 ± 219	539 ± 408	3818 ± 938	26
7	D0260101	HD113708	304.55	-2.39	8830 ± 2995	9228 ± 2450	6640 ± 2010	20065 ± 2188	20591 ± 2444	6780 ± 2126	107
8	D0260102	HD113708	304.55	-2.39	5304 ± 3078	7611 ± 2093	6627 ± 5022	14273 ± 3724	11357 ± 2194	5788 ± 4386	107
9	D0260201	HD113659	304.52	-2.26	7544 ± 4087	7254 ± 1815	6468 ± 3903	13014 ± 3199	10914 ± 1836	4074 ± 3087	120
10	D0260301	HD111641	302.97	-3.98	3647 ± 2339	6132 ± 1319	3031 ± 518	13779 ± 2020	10584 ± 1736	3461 ± 674	53
11	D0260302	HD111641	302.97	-3.98	8422 ± 2586	8733 ± 1547	12287 ± 3606	14065 ± 2035	13242 ± 1723	4803 ± 2941	53
12	D0260401	HD111195	302.65	-4.49	5772 ± 2082	8091 ± 1472	8838 ± 1693	10249 ± 1482	10459 ± 1473	7687 ± 1814	62
13	D0260402	HD111195	302.65	-4.49	8194 ± 2188	10160 ± 1561	10778 ± 1576	9044 ± 1419	8583 ± 1990	11029 ± 1790	62
14	D0260501	HD111283	302.69	-2.72	6666 ± 4015	9077 ± 2191	6648 ± 5038	12683 ± 2164	15342 ± 3167	7048 ± 4859	83
15	D0260601	HD116796	306.94	-0.95	4338 ± 2510	4139 ± 1650	4627 ± 3506	4827 ± 897	3119 ± 2364	3791 ± 2708	203
16	D0260701	HD117667	299.95	-2.73	23614 ± 5031	22132 ± 4400	16511 ± 6952	13621 ± 3080	14986 ± 4366	12930 ± 6116	67
17	D0260702	HD117667	299.95	-2.73	9626 ± 4093	12149 ± 2720	... [c]	10161 ± 2827	4667 ± 3537	... [c]	67
18	E0290101	Coalsack-1	303.52	-1.32	8926 ± 1725	11212 ± 824	10515 ± 1375	10976 ± 1073	9025 ± 999	7224 ± 1637	235
19	E0290301	Coalsack-3	297.02	-3.62	3678 ± 2787	5685 ± 1544	5389 ± 3621	13792 ± 2019	13043 ± 1994	3147 ± 2385	64
20	E0290401	Coalsack-4	308.01	-4.99	4216 ± 2278	5957 ± 1067	3741 ± 2163	5487 ± 1379	4861 ± 1544	3024 ± 1669	46

Table 1—Continued

No.	Data ID	Target Name	l (deg)	b (deg)	Observed UV Intensity ± Error (photons cm^{-2} s^{-1} sr^{-1} Å^{-1}) 1A1 (1004 Å)	1A2 (1058 Å)	2A2 (1112 Å)	1B1 (1117 Å)	1B2 (1157 Å)	2A1 (1159 Å)	IR 100 μm (MJy sr^{-1})
21	S4050701	HD96548-BKG	292.32	-4.83	7051 ± 766	9408 ± 1521	8270 ± 2461	9441 ± 1667	8141 ± 1284	8979 ± 1148	53
22	S4051701	HD104994-BKGD	297.56	0.34	10005 ± 1305	12378 ± 796	17134 ± 1162	11626 ± 878	11241 ± 980	11823 ± 1318	258
23	S4055301	WR42-HD97152-BGD	290.95	-0.49	660 ± 500	1288 ± 541	3031 ± 518	144 ± 109	360 ± 273	3461 ± 674	267
24	S4055801	HD102567-BKGD	295.61	-0.24	3538 ± 1256	5279 ± 455	1767 ± 527	3452 ± 690	3206 ± 849	5330 ± 915	266
25	S4059101	HD104994-BKGD	297.56	0.34	8711 ± 1056	10994 ± 589	11305 ± 1059	9852 ± 693	8971 ± 618	9659 ± 715	258
26	S5052801	HD108002-BKGD	300.16	-2.48	10808 ± 3230	17048 ± 1309	16862 ± 3320	13498 ± 2022	11437 ± 2069	13198 ± 3158	68
27	S5059001	POLE-BKGD	307.12	-2.44	1953 ± 1359	5221 ± 682	7151 ± 2213	4157 ± 981	6476 ± 868	2498 ± 1317	78
28	S5059101	POLE-BKGD	303.9	-8.14	1458 ± 724	4522 ± 565	5985 ± 1032	4019 ± 488	3646 ± 927	2136 ± 1042	20
29	S5059102	POLE-BKGD	303.9	-8.14	1707 ± 1294	4872 ± 1622	2044 ± 1549	2134 ± 1617	1985 ± 1304	2213 ± 1677	20
30	S5059201	POLE-BKGD	301.97	-2.14	10641 ± 1674	13708 ± 845	16677 ± 1393	10501 ± 829	9378 ± 924	8117 ± 1940	60
31	S5059302	POLE-BKGD	298.92	-8.51	2792 ± 1513	4377 ± 1359	4769 ± 2393	4441 ± 1428	2767 ± 1501	1645 ± 849	12
32	S5160101	HD104994	297.56	0.34	8475 ± 1395	12669 ± 695	15611 ± 1863	11667 ± 884	10333 ± 931	12731 ± 1245	258
33	S5058901	POLE-BKGD	308.54	-8.86	645 ± 489	2220 ± 515	4948 ± 1169	3980 ± 550	3918 ± 652	4156 ± 928	14
34	S5058902	POLE-BKGD	308.54	-8.86	1155 ± 875	2001 ± 710	1958 ±1448	3046 ± 851	2699 ± 978	1118 ± 847	14

[a]Murthy et al. (1999)

[b]Murthy et al. (1994)

[c]Data nonexistent

Table 2. *FUSE* WAVELENGTH BANDS

Detector	bands	Wavelength range (Å)	Average Wavelength (Å)
LiF	1A1	987.1 - 1020.8	1004
LiF	1A2	1034.8 - 1081.4	1058
LiF	2A2	1095.0 - 1128.6	1112
LiF	(2A2+1B1)/2*		1114
LiF	1B1	1100.3 - 1133.7	1117
LiF	1B2	1133.7 - 1180.1	1157
LiF	(1B2+2A1)/2*		1158
LiF	2A1	1142.0 - 1175.3	1159

*Derived band

Table 3. BRIGHTEST STARS IN THE REGION

HD Number	Name	l (deg)	b (deg)	Sp. Type[a]	Distance[a] (pc)	Luminosity[b] at 1100 Å (photons s^{-1} $Å^{-1}$)
122451	β Cen	311.77	1.25	B1III	161.3	2.45×10^{46}
108248	α Cru	300.13	-0.36	B0.5IV	98.3	1.28×10^{46}
111123	β Cru	302.46	3.18	B0.5IV	108.1	1.0×10^{46}
93030	θ Car	289.6	-4.9	B0Vp	134.6	4.62×10^{45}
104841	θ Cru	297.64	-0.78	B2IV	230.9	1.38×10^{45}
99264		296.32	-10.51	B2IV-V	271.0	1.17×10^{45}
91465	PP Car	287.18	-3.15	B4Vne	152.4	6.87×10^{44}
102776	J Cen	296.18	-1.73	B3V	140.9	3.45×10^{44}
92938	V518 Car	289.56	-5.00	B3V	139.9	2.29×10^{44}
93607		289.97	-4.69	B3IV	137.7	1.95×10^{44}
103884	Glazar Cru 135	296.76	-0.22	B3V	183.5	1.77×10^{44}
93194		289.50	-4.46	B5Vn	148.4	6.61×10^{43}
99103		293.78	-3.66	B5	145.6	6.00×10^{43}

Note. — Stars in descending order of UV luminosity

[a]From Hipparcos Catalog (Perryman et al. 1997)

[b]Using Kurucz Model scaled to V magnitude.

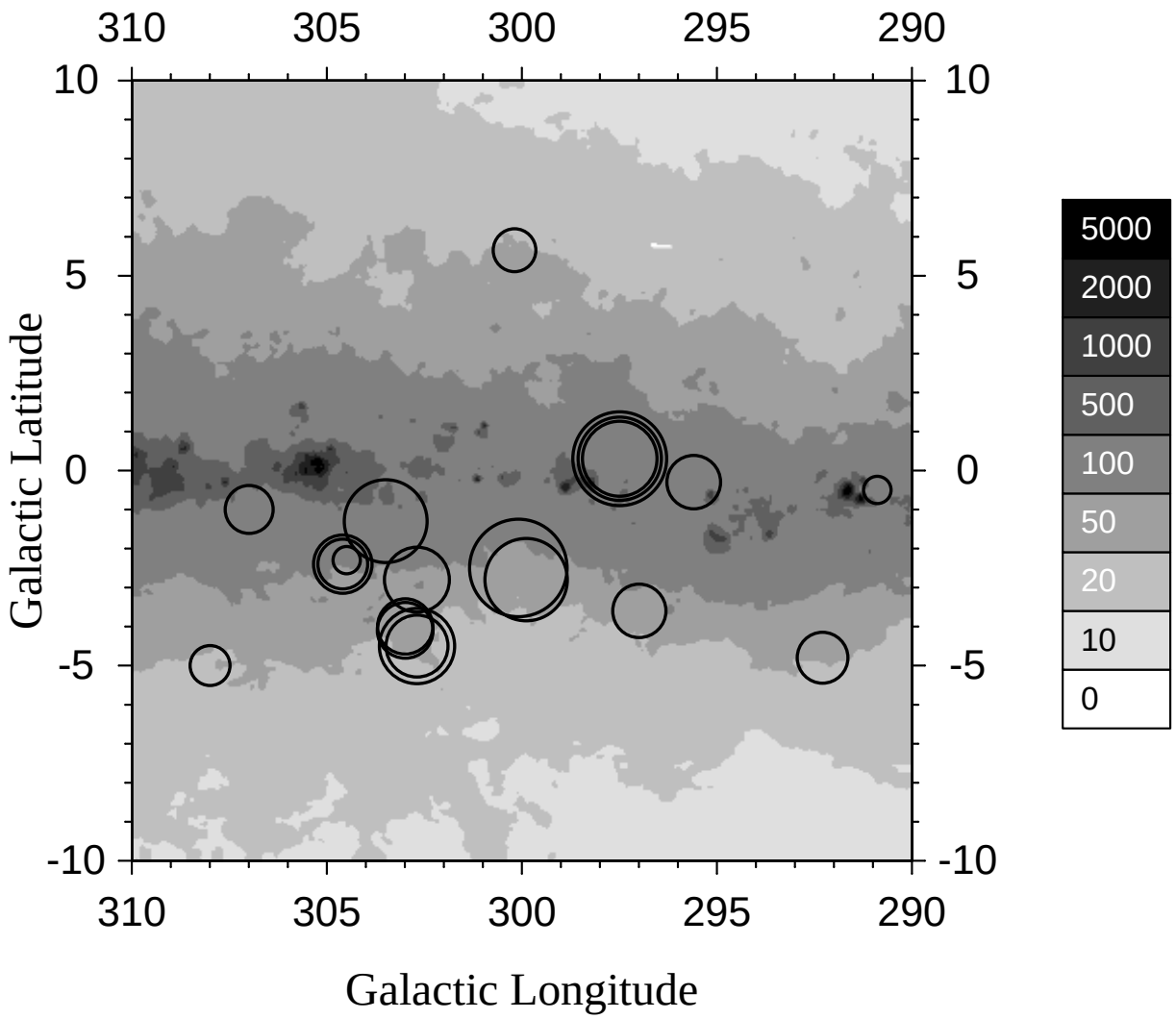

Fig. 1.— IRAS 100 μm (in units of MJy sr^{-1}) map of the region is plotted with the observed locations marked as circles whose diameter is proportional to the weighted average intensity of the 2A2 and 1B1 bands (1114 Å) in units of photons cm^{-2} s^{-1} sr^{-1} Å^{-1}.

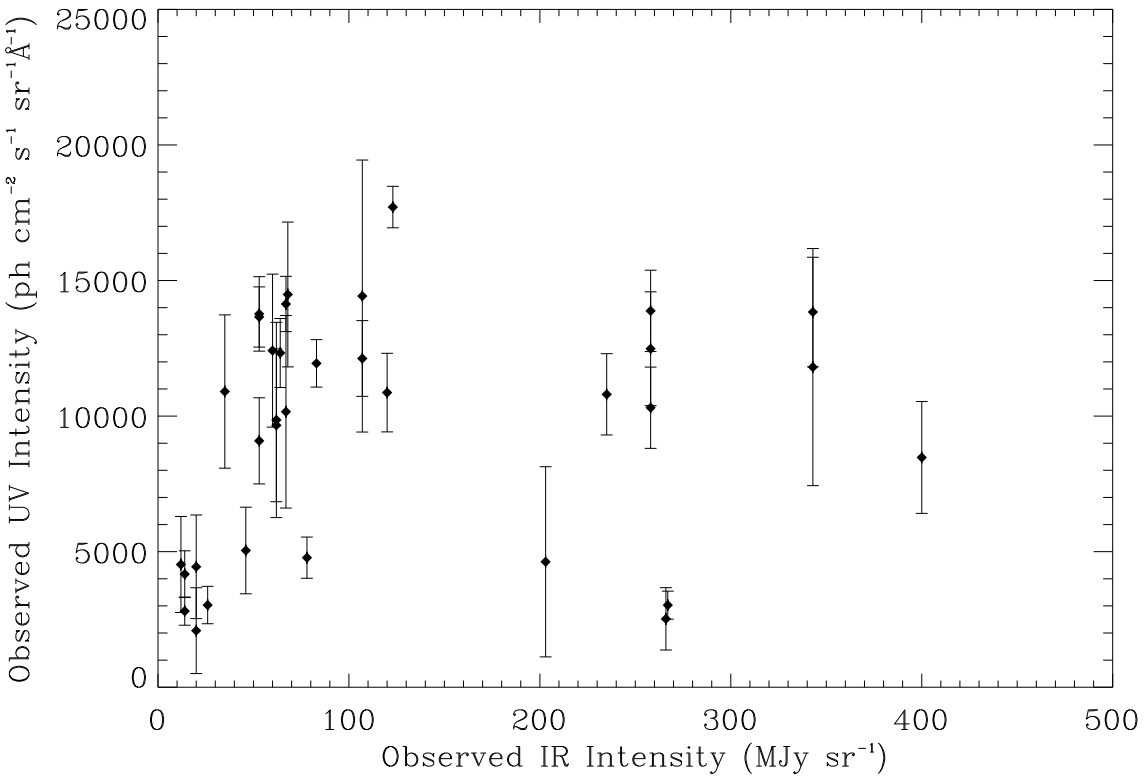

Fig. 2.— Weighted average UV intensities of 2A2 and 1B1 bands (1114 Å) with 1σ error bars are plotted against the observed IRAS 100 μm intensities at each location.

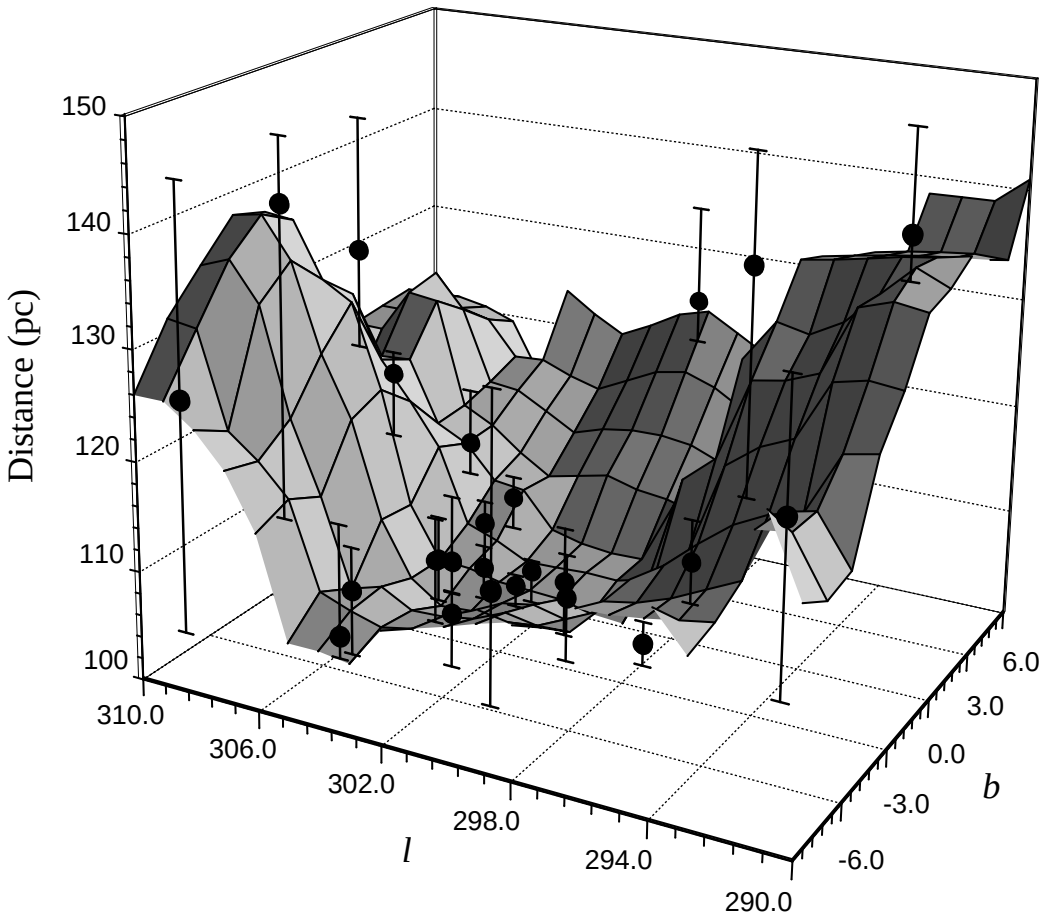

Fig. 3.— Best fit distance of the more distant of the two H I clouds (derived from the weighted average intensities of 2A2 and 1B1 bands at 1114 Å, assuming that a and g remain constant throughout the region) is shown as dark circles with error bars showing the range of allowed distances. The interpolated surface fit for the region is also overplotted.

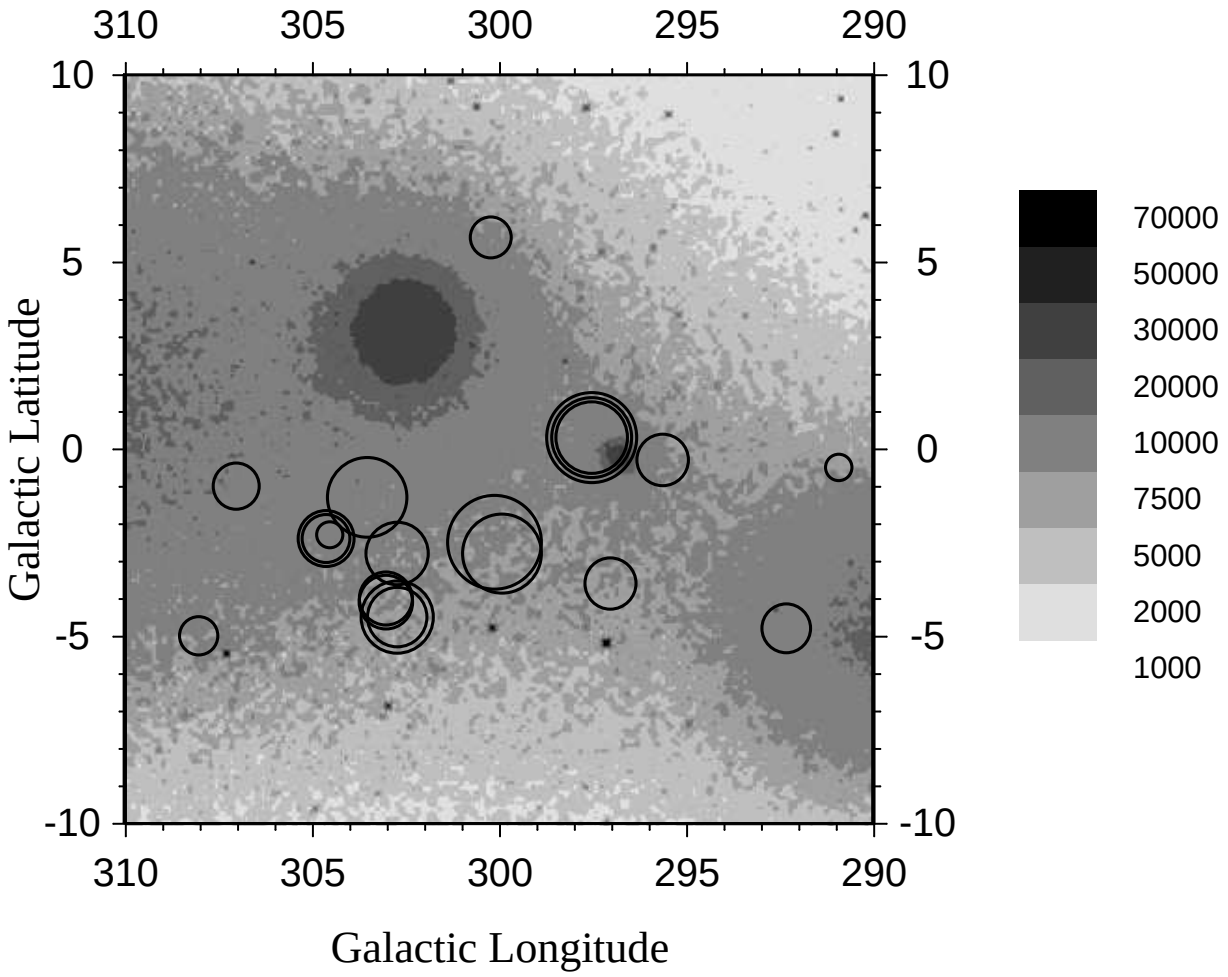

Fig. 4.— The scattered light predicted by our model with $a = 0.28$ and $g = 0.61$ is shown in figure in units of photons cm^{-2} s^{-1} sr^{-1} Å^{-1}. The observed locations are overplotted as circles whose radii are proportional to their intensity at 1114 Å.

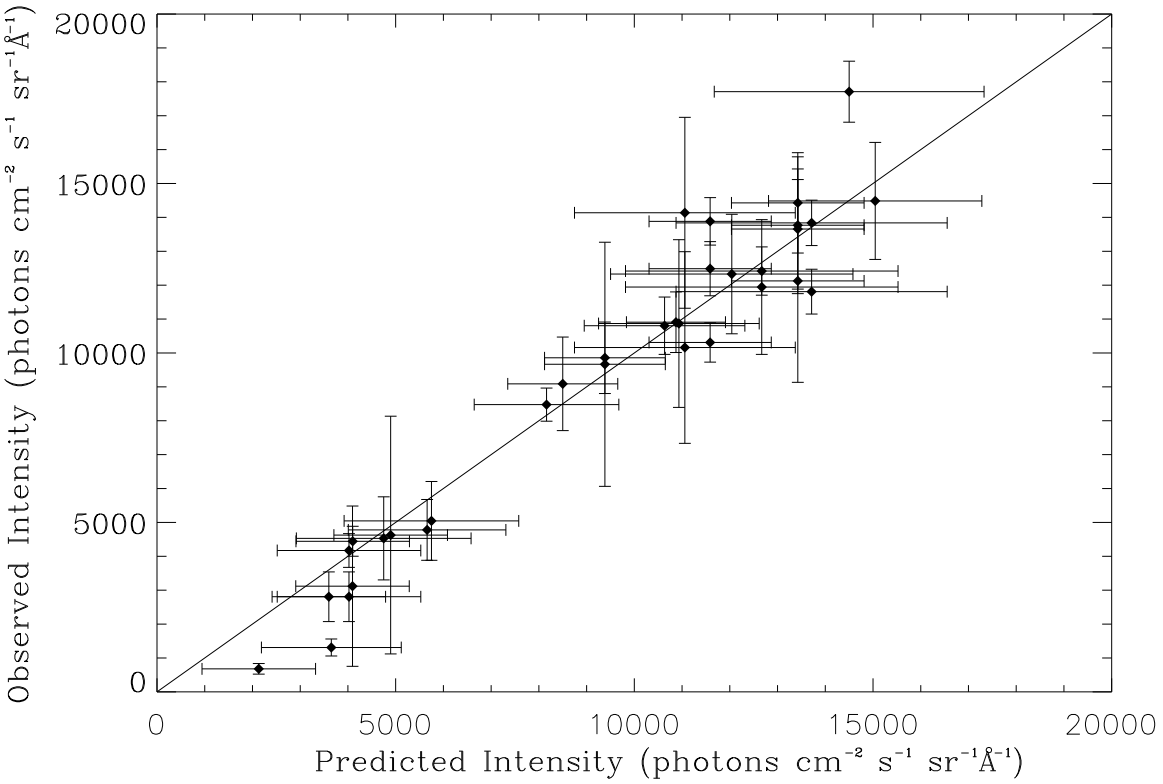

Fig. 5.— The weighted average intensities of the 2A2 and 1B1 bands (1114 Å) have been plotted against the predicted UV intensities at 1114 Å with $a = 0.28$ and $g = 0.61$. The vertical error bars represent observational errors while the horizontal error bars represent model uncertainties.

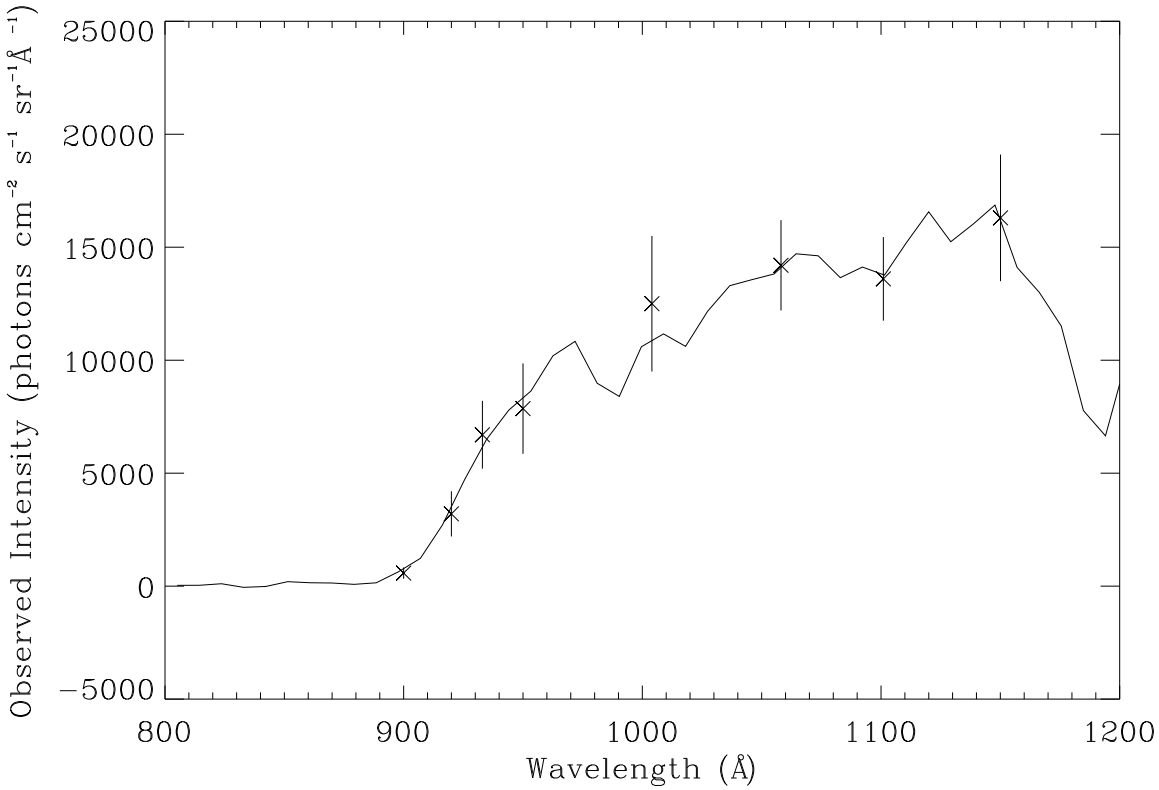

Fig. 6.— Predicted intensities corresponding to the best fit parameters are shown as stars on a *Voyager* observation (No. 2 in Table 1). The error bars correspond to the range allowed by the uncertainty in the optical constants.

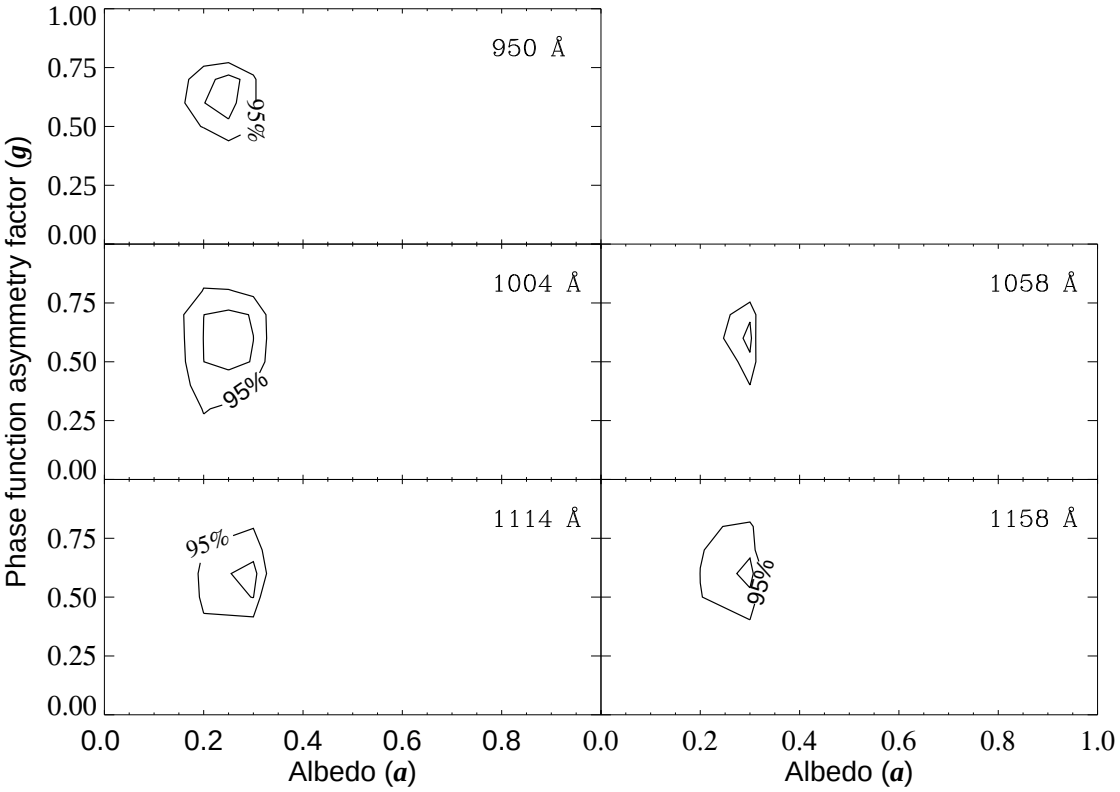

Fig. 7.— 67% and 95% confidence contours (g versus a) are plotted for wavelengths 950, 1004, 1058, 1114 & 1158 Å. Only the 5 *Voyager* observations could be used to constrain the derived values at 950 Å.

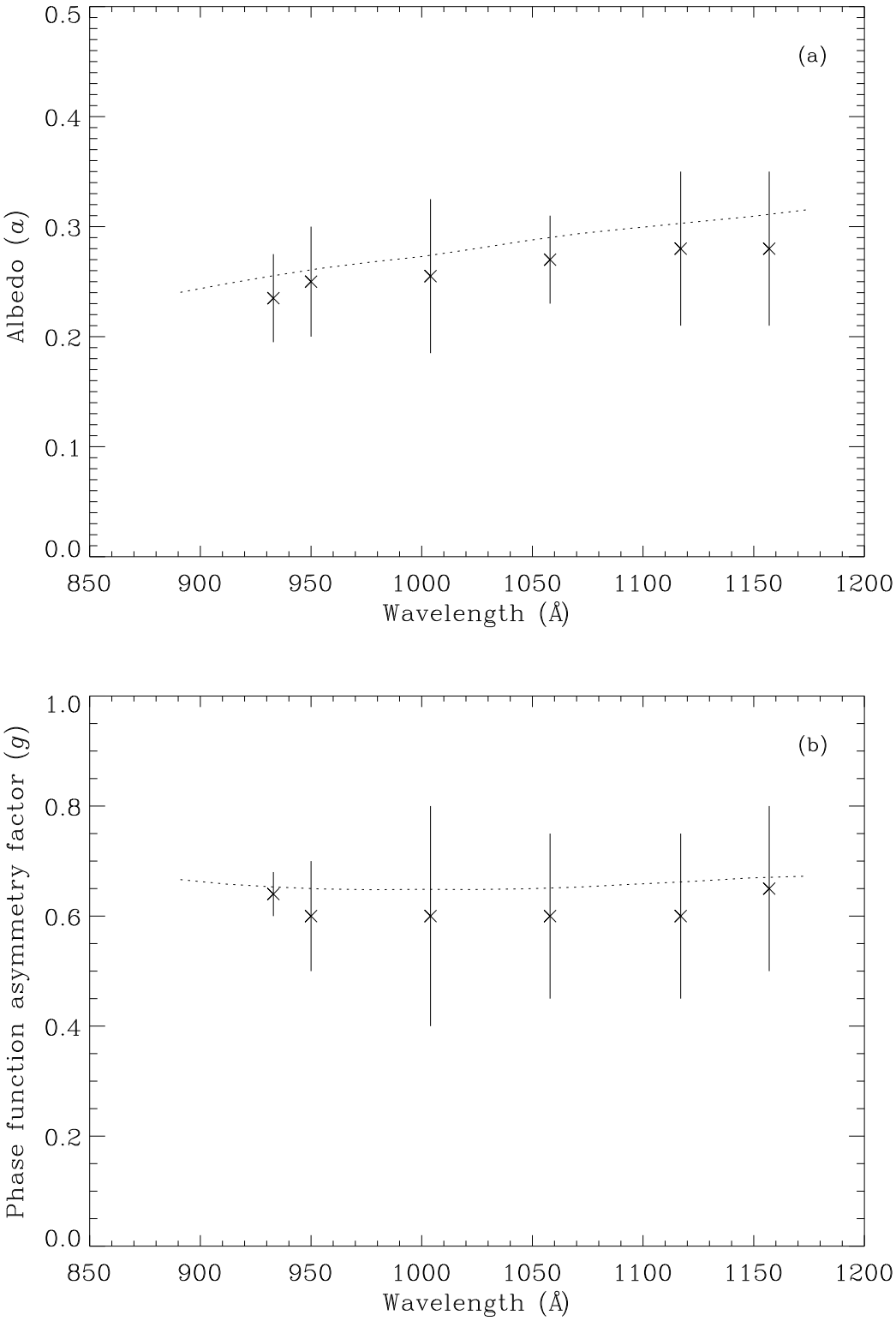

Fig. 8.— The spectral variation in the albedo a and in the phase function asymmetry factor g are plotted in (a) and (b), respectively. The theoretical prediction of Weingartner & Draine (2001) is overplotted as dotted line.